AASCIT Journal of Materials
2018; 4(4): 19-32
http://www.aascit.org/journal/materials
ISSN: 2472-9736 (Print); ISSN: 2472-9752 (Online)

American Association for Science and Technology

Keywords
Contraction of Phase,
Dislocation,
Microstructure

Received: January 8, 2018
Accepted: January 22, 2018
Published: February 12, 2018

Theory Regarding Precipitation of Carbides During Deep Cryogenic Treatment of 45WCrV7 Tool Steel

Seyed Ebrahim Vahdat[1, *], Keyvan Seyedi Niaki[2], Ali Mohamadinia[1]

[1]Department of Engineering, Ayatollah Amoli Branch, Islamic Azad University, Amol, Iran
[2]Department of Mechanical Engineering, Iranian Research Organization for Science and Technology (IROST), Tehran, Iran

Email address

e.vahdat@iauamol.ac.ir (S. E. Vahdat)
[*]Corresponding author

Citation

Seyed EbrahimVahdat, Keyvan Seyedi Niaki, Ali Mohamadinia. Theory Regarding Precipitation of Carbides During Deep Cryogenic Treatment of 45WCrV7 Tool Steel. *AASCIT Journal of Materials.* Vol. 4, No. 1, 2018, pp. 19-32.

Abstract

Longer cryogenic holding times may decrease the amount of retained austenite and thus increase the amount of carbon available for carbide formation. However, in the case of there isn't retained austenite in the microstructure, what is the origin and where is appropriate places of the formation of carbide in cryogenic treatment? In this research, first, theoretical study has been done by thermodynamic phenomenon. Second, nine sets of 45WCrV7 tool steel specimens have been deep cryogenic treated and then tempered. After that, experimental study has been done by double deep cryogenic treatment in all sets. Result was: In terms of thermodynamics, deep cryogenic temperature provided the possibility for the formation of 1.55×10^{17} m/m^3 dislocations around the primary carbide with diameter of 2µm which they are facilitate the formation of carbide during tempering. In terms of experiment, in deep cryogenic treatment and during tempering, new carbides precipitated around primary carbides obviously.

1. Introduction

Normally, increase in strength and wear resistance of tool steels is associated with a reduced modulus of toughness. However, DCT may be used to simultaneously increase tensile strength and hardness and improve modulus of toughness of tool steels. Effects of different DCT cycles on mechanical properties of 45WCrV7 tool steel have been studied previously by Authors. Several sets of specimens were investigated: three sets of untreated specimens, for studying the effect of some hardening parameters on the metal properties, and nine sets consisting of DCT specimens. Soaking and tempering temperatures were kept constant at -196°C and 200°C, respectively. Different DCT cycles were implemented by varying soaking time (24, 36 and 48 h) and tempering duration (60, 120 and 180 minutes). In order to ensure optimum treatment conditions, time gaps between various treatment steps were kept to minimum. Results show that two DCT cycles consisting of: (i) 36 h soaking at -196°C and 1 h tempering at 200°C, and (ii) 48 h soaking at -196°C and 2 h tempering at 200°C produce the best effects in the DCTed 45WCrV7 tool steel specimens, namely 32-36% increase in tensile strength, 9-12% increase in hardness, and 12-35% improvement in modulus of toughness. The precipitation of secondary carbides was responsible for that. This research focuses on the mechanism of this improvement.

The first mechanism of precipitation of secondary carbide is due to the expansion

resulting from transformation of the retained austenite into martensite and secondly caused by the difference in thermal contraction of the phases [1]. No theoretical and experimental study has been done on the second mechanism. Therefore, this research will fill a portion of this knowledge gap.

1.1. First Mechanism

Li et al. [2-8] investigated internal friction behavior in DCT of steel containing 0.91wt% carbon, 8.6wt% chromium, 1.47wt% molybdenum, 0.51wt% silicon, and 0.3wt% vanadium. Their investigation showed that, in DCT, the expansion caused by the transformation of retained austenite into martensite led to the formation of very fine secondary carbide precipitations during the tempering. Carbon atoms were absorbed by the closest dislocations, which ultimately led to high-density carbon regions around the dislocations. So, at lower tempering temperatures, appropriate regions were formed for the secondary carbide formation at 495 K (approximately 220°C). Since carbon atom movement does not occur at very low temperature, in-situ studies on the internal friction behavior of two types of high-alloy tool steels with 10-12wt% alloy and 0.9-1wt% carbon in DCT showed that the carbon atom did not move, but dislocation gliding or dislocation dragging in the direction of dislocation pipe [9] led to the arrangement of dislocations with the interstitial carbon atoms. The required energy for dislocation slip was provided via the strain energy caused by contraction at DCT temperature. Then, during tempering, by moving carbon by a fraction of atomic distance, the secondary carbide was formed. Also, Liu et al. showed that, in DCT, high-chromium cast-iron 3Cr13Mo1V1.5 with the equivalent carbon of less than 2.06wt% (containing 2.82wt% carbon, 13.34wt% chromium, 2.8wt% manganese, 1.5wt% vanadium, 0.7wt% molybdenum, and 1.24wt% silicon) was in super-saturation mode of austenite and martensitebecause of the presence of approximately 2.8wt% carbon. For example, carbon content of martensite in DCT sample was 0.10wt%, while it was 0.21wt% in the as-cast sample [10, 11]. Therefore carbon segregation occurred. This led to the formation of very fine secondary carbide precipitations during the tempering.

During carbonsegregation, carbon atom needs to move, even as small as possible, which is almost impossible at very low temperature, e.g. -196°C. Therefore, Tyshchenko et al. [12] showed that, in X220CrVMo13-4 tool steel with the equivalent carbon of less than 2.06wt% (containing 2.2wt% carbon, 0.13wt% chromium, 4wt% vanadium, and 1wt% molybdenum), during the DCT, plastic deformation occurred as a result of the expansion caused by the transformation of retained austenite into martensite. Thus, these tensions led to dislocation creep. The plastic deformation in the matrix increased dislocation density and transferred non-moving carbons through the slip of dislocations. Results of internal friction measurements in liquid nitrogen reinforced the carbon decoration idea on dislocations during dislocation dragging at very low temperature [12]. In longer DCT times, the only absorbing factor for non-moving carbons toward dislocations was the slip of dislocations via plastic deformation or the resulting tensions and ultimately dislocations creep.

These three research groups [2-8, 10-12] have admitted that the increased volume caused by the transformation of retained austenite into martensite is the cause for the formation of secondary carbide precipitation. However, in DCT, in which retained austenite has not change, the secondary carbide is formed over the DCT time. For example, in Das et al.'s study [13, 14], austenite was completely transformed into martensite via the DCT of AISI D2 tool steel. But, in longer DCT times up to 72 hours; the content of secondary carbide was increased from 7.5wt% to 10 wt%. Another example in Prieto et al.'s work [15] was that, in the DCT of AISI 420 stainless steel containing 0.177 wt% carbon and 12.83 wt% chromium, the microstructure of all the samples lacked the retained austenite. Nevertheless, in longer DCT times, content of secondary carbide was increased by almost two-fold.

The question is as follows: In the absence of the transformation of the retained austenite into martensite, what is the mechanismof the formation of secondary carbide in DCT? The present research tried to answer this issue.

1.2. Second Mechanism

The first mechanism of precipitation of secondary carbide is due to the expansion resulting from transformation of the retained austenite into martensite during DCT [2-8, 10-12, 16]. There are a lot of considerations about the effects of high carbon- high alloy steels. Conversely, the medium carbon-low alloy steel studied by this research contains 0.48wt% carbon and 3.7 wt% alloy elements. This makes a significant difference in the microstructures of steel between their research and present study. The composition given in Table 1 suggests that this is a low alloy, shock resistant (type S1) tool steel. Therefore, the use of a liquid nitrogen quench is likely needed to transform all austenite to martensite, due to its low alloy and medium carbon contents.

Hoyos et al. [17], accompanied by some other researchers [18, 19], expressed that Li et al. [2-8] ignored the influence of dislocation density variations, because in both of the specimens (quenched+DCT and quenched + non-DCT), with increasing austenite temperature from 1273 to 1313 and then to 1353 K, height of internal friction peak at 583 K increased. This phenomenon was related to the high content of interstitial carbon in martensite, while increased peak height can be caused by increased dislocation density.

In the second mechanism, primary carbide can be considered as a phase that it has different thermal expansion coefficient from the matrix. So, population density of secondary carbide particles should be much higher around them. No theoretical and experimental work has been showed for validating this theory. This paper presents our work for filling up some of this knowledge gap by using XRD, FESEM and STEM.

2. Theory

In steels contain up to 0.4 wt% carbonmartensite takes the form of laths rather than plates after quenching. A typical lath has dimensions 0.3×4×200 µm. In addition, butterfly martensite forms at the highest temperatures, lenticular martensite forms at intermediate temperatures, and thin-plate martensite forms at the lowest temperatures [20, 21]. Chemical composition of 45WCrV7 too steel contains 0.48 wt% carbon and 2.7 wt% W and Cr. Therefore martensite takes the form of thin-plate rather than other morphology of martensite after DCT. Figure 1 shows the initial austenite (red lines) transform to thin-plate martensites (whitelines) after quenching and DCT. After tempering, thin-plate martensites (whitelines) transform to thin-plate ferrite (whitelines) and precipitated carbides (yellow arrows).

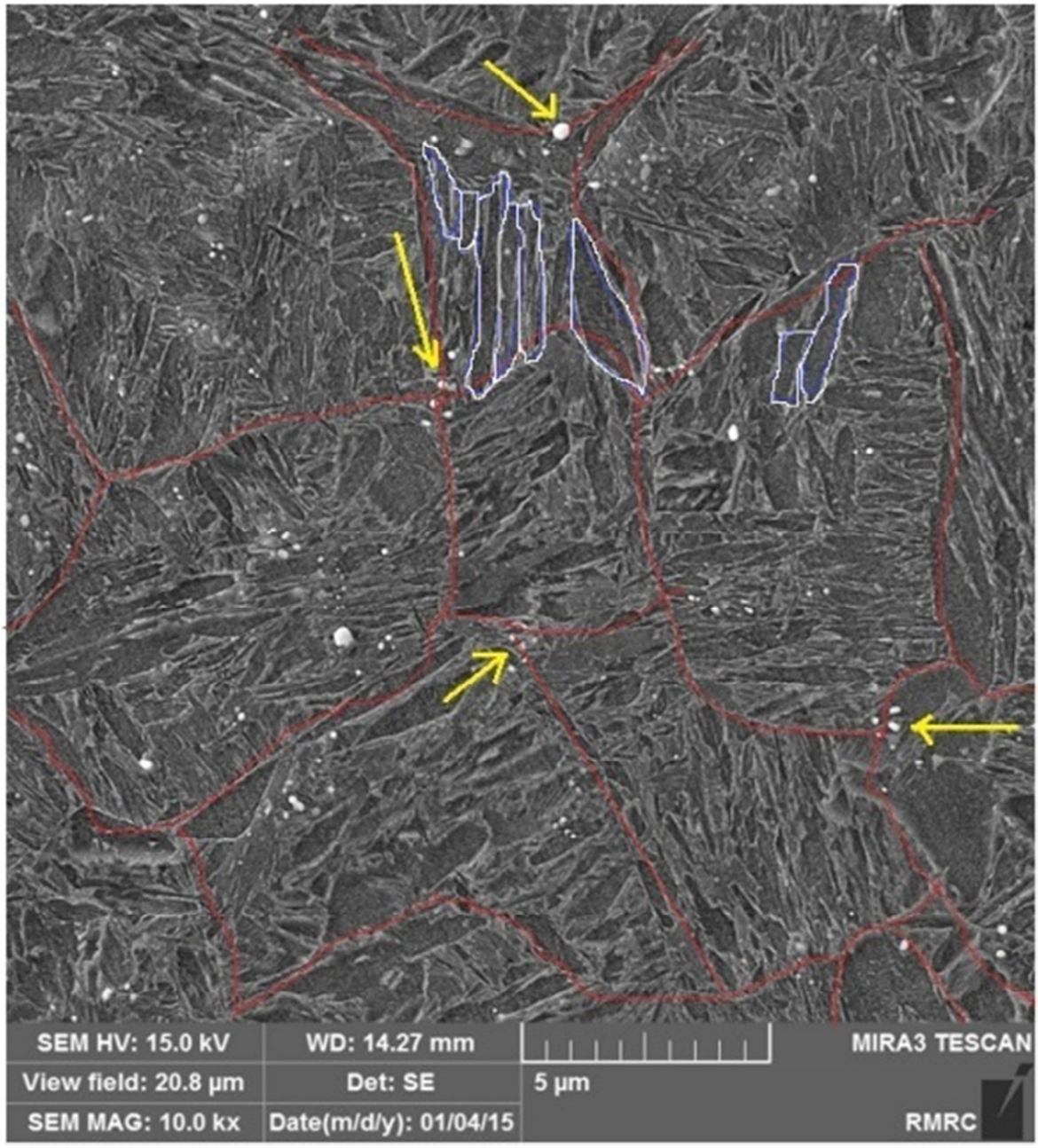

Figure 1. *Initial austenite (red lines), thin-plate ferrite (blue lines) and precipitated carbides (yellow arrows) by using FESEM.*

Unlike the plate morphology which typically contains a high density of transformation twins, thin-platesmartensite are typically untwinned and contain a high density of internal dislocations. Since the inhomogeneous shear in ferrous thin-plate martensite is not twinning, it is expected that slip (drag) is the mode involved and that the lattice-invariant deformation would be effected by the movement of interface dislocations [20-25]. Figure 2 shows STEM of dislocations like as dark squiggly lines after DCT.

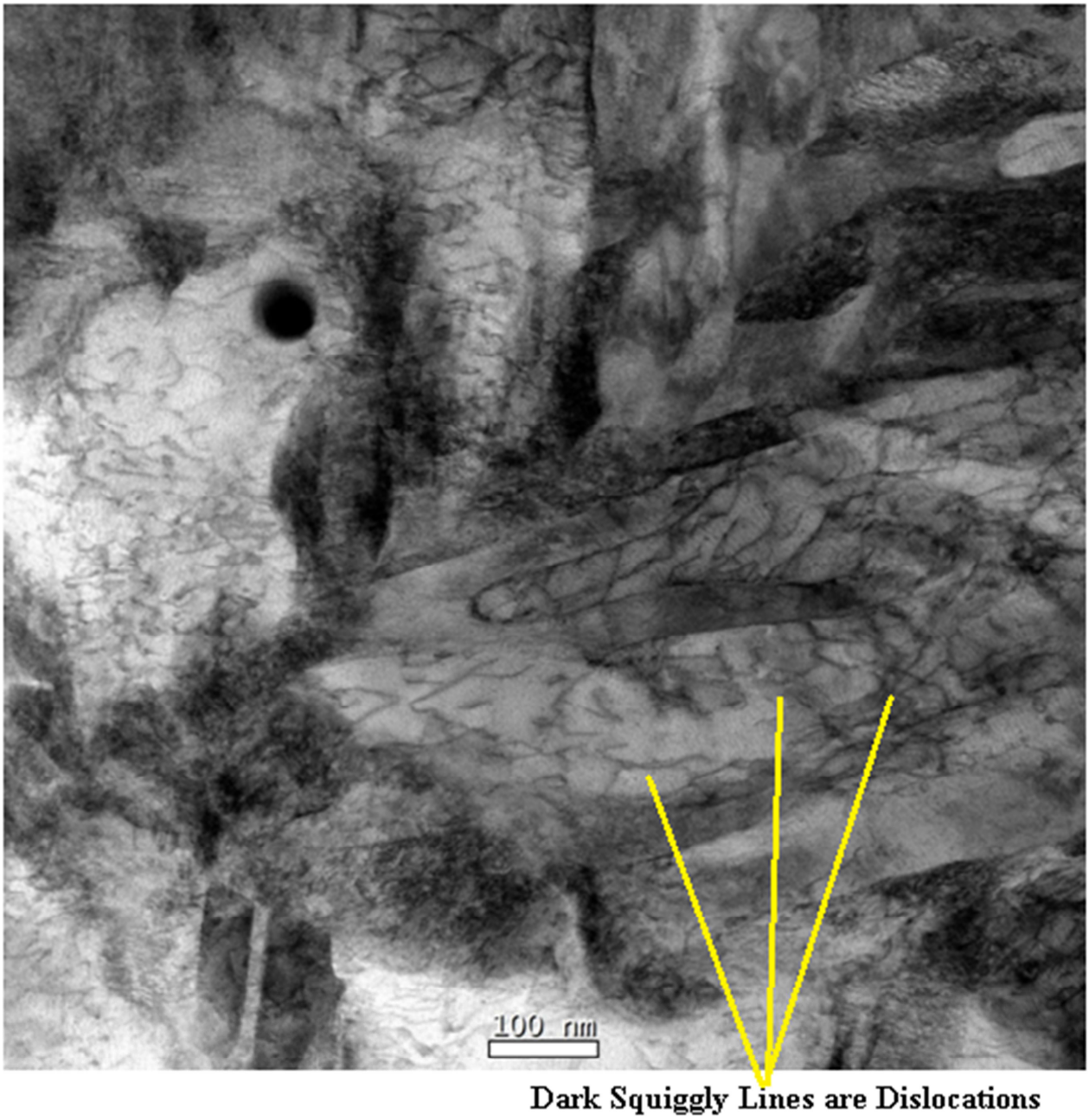

Figure 2. *Dislocations in 45WCrV7 tool steel after DCT by using STEM.*

Second mechanism of precipitation of carbide in the 45WCrV7 tool steel indicated that, at DCT, physical changes in the matrix and primary carbide (for example M_7C_3) led to create dislocations. Now, the question is "as a result of difference in contraction of matrix and primary carbide, is the energy required for dislocation formation provided in the surrounding areas of primary carbide?"

To answer this question, first maximum energy required for the formation of one dislocation in an iron crystal (E_d) was estimated. Then, minimum energy obtained from physical changes between matrix and primary carbide was calculated at 77K (E_Δ). $E_d \leq E_\Delta$ should be established in order for the preferred places of precipitation of carbide to be thermodynamically performed.

Energy of one dislocation is equal to the work required for moving crystal plates as much as Burger's vector size (b). For crystal of iron with $\nu = 0.3$, edge dislocation energy is 1.43 times larger than screw dislocation because $E_{edge}/E_{scrow}=1/(1-\nu)$. The amount of energy for edge dislocation per unit of edge dislocation length can be obtained from the Equation (1) [26].

$$E_{edge}= G\times b^2\times Ln(R/r)/ (4\pi\times(1-\nu)) \quad (1)$$

G is shear modulus of matrix for body centered cubic iron crystal with cubic constant of 0.2866 nm equal to 79.3GPa.

b is length of Burgers' vector for body centered cubic iron crystal with cubic constant of 0.2866 nm equal to $b=\sqrt{3}\times a/2=0.25$nm.

r is radius of dislocation core. In the center of dislocation, there is severe distortion and high strain; therefore, Hooke's law is not established. So, r≥5b is considered to establish Hooke's law.

R is radius of dislocation cylinder. In fact, maximum amount of R can be considered as half of the distance between two dislocations. If, in the annealed iron crystal, population density of dislocation is assumed to be 10^6 per mm^2, distance of two dislocations will become the inverse of square root of density of dislocation, i.e. 10^{-3}mm (or 1 μm). So, in this state, maximum size of R will be 0.5 μm.

υ is Poisson of matrix (iron crystal) equal to 0.3.

In iron crystal, $G=79.3\times10^9$ Pa, $b=\sqrt{3}\times a\div2=0.25$ nm, r=5b=1.25 nm and R=0.5μm. Edge dislocation energy per unit length of edge dislocation is equal to 3.38nJ. So, maximum energy required for forming one edge dislocation with length of 1000r =1000×5b=5000b=1250nm (length of a dislocation is usually considered 1000r) is almost equal to 4×10^{-15}J.

System is an area in the matrix around primary carbide. It is studied whether this area provides the energy required for forming dislocation or not. Energy resulted from reducing temperature in the system is divided into two parts. The first part is inner energy (U) and second is multiplication of pressure by volume (P.V). In this system, energy changes are divided to three parts. The first part is the energy caused by the system's thermal capacity; second part is the energy resulted from the system's volume changes and the third part is the energy of the system's pressure changes. In fact, in the third part, energy results from stress caused by the difference in volume of primary carbideand matrix as a result of contraction.

In this research, maximum size of primary carbidewas 2 μm. System was considered the area surrounding these particles, a ring with internal diameter of 2 μm and external diameter of 2.5 μm. Therefore, V is volume of the area around primary carbide, i.e. the system was equal to 4×10^{-18} m^3.

In this research, volume of primary carbide with an almost spherical shape with maximum diameter (D) of 2 μm was equal to $4.19\times10^{-18}m^3$.

Iron density was equal to 7860 kg per m^3 and density of primary carbide (M_7C_3) was 6900 kg per m^3.

α_v is coefficient of thermal expansion in three dimensions, α_L is coefficient of thermal expansion in one dimension, $\alpha_{L,M7C3}$ is coefficient of thermal expansion for primary carbide equal to 10^{-5} K^{-1} and $\alpha_{L,Fe}$ is coefficient of thermal expansion for iron matrix and equal to 1.5×10^{-5} K^{-1}. Coefficient of thermal expansion for primary carbide with hexagonal structure was not isotropic. This amount was 1.336×10^{-5} K^{-1} in directiona and 0.869×10^{-5} K^{-1} in direction c, which was considered 10^{-5} K^{-1} for isotropic simplification. Coefficient of thermal expansion was given at 20°C. At deep cryogenic temperatures, its changes were negligible.

dT is temperature decrease from room temperature to temperature of liquid nitrogen and equal to dT=77K-297K=-220 K.

E is Young's modulus of iron matrix, equal to 200 GPa; Young's modulus of primary carbide (M_7C_3) is equal to 245 GPa.

e is strain as a result of difference in contraction of primary carbide and iron matrix.

C is thermal capacity. Thermal capacity of iron at room temperature and pressure of 1 atmosphere is equal to 449 J/kg.K. Thermal capacity of primary carbide(M_7C_3) in the same conditions is equal to 630 J/kg.K. At deep cryogenic temperatures, changes of thermal capacity were negligible; therefore, it was considered constant.

At deep cryogenic temperature (77 K), Entropy changes can be neglected. The amount of iron Entropy at room temperature was 27 J/(mol.K). As a result, the energy derived from temperature reduction in the system was equal to -198760×10^{-14}J.

Maximum energy required for forming one dislocation (equal to 4×10^{-15}J) was much less than the energy (equal to -198760×10^{-14} J) obtained from temperature reduction in the mentioned parts around primary carbide in iron matrix. Thus, in terms of thermodynamic, DCT provided the possibility for the formation of 496900 dislocations with 1250 nm length around the primary carbide with diameter of 2 μ into volume of 4×10^{-18} m^3. Volume population density of dislocation calculated as $496900\times1250\times10^{-9}/(4\times10^{-18})=1.55\times10^{17}$ m/m^3. As a result, stored energy caused by the difference in the thermal expansion coefficient between of primary carbide and matrix is $1.55\times10^{13}cm/cm^3\times4\times10^{-15}J \div 0.000125$ cm ≈ 496 J/cm^3.

Typical energies associated with martensitic transformation (the sum of strain energy, twin interface energy, austenite-martensite interface energy and stored energy due to dislocations) is about 155 J/cm^3 (1100 J/mol) for low alloy steels [20-22]. In this theory, stored energy is about 496 J/cm^3 caused by the difference in the thermal expansion coefficient between of primary carbide and matrix of 45WCrV7 low alloy tool steel. Thus, in terms of thermodynamic, DCT provided the possibility for the formation new carbides.

The barrier energy is 8×10^{-16} J for per martensite nucleation event where the transformation typically occurs for low alloy steels [22, 23]. In this theory, the energy derived for temperature reduction in the mentioned parts around primary carbide in iron matrix was equal to 1.98760×10^{-9} J. It is much higher than the barrier energy mentioned above. Therefore it is frequently thought that dislocation arrays serve as carbide nuclei during tempering.

For summary, the second mechanism of precipitation of carbides is due to the difference in contraction coefficient between primary carbide and matrix at deep cryogenic temperatures, a tension stress occurs. It illustrated in Figure 3. The resulting tension stress produces a dislocation loop around the primary carbide. By the passage of time in the DCT, the dislocation loops expand by dislocation creep. During tempering, the carbon atoms move as a fraction of atomic distances to decorate the dislocations. Therefore the conditions for forming the new carbides facilitate.

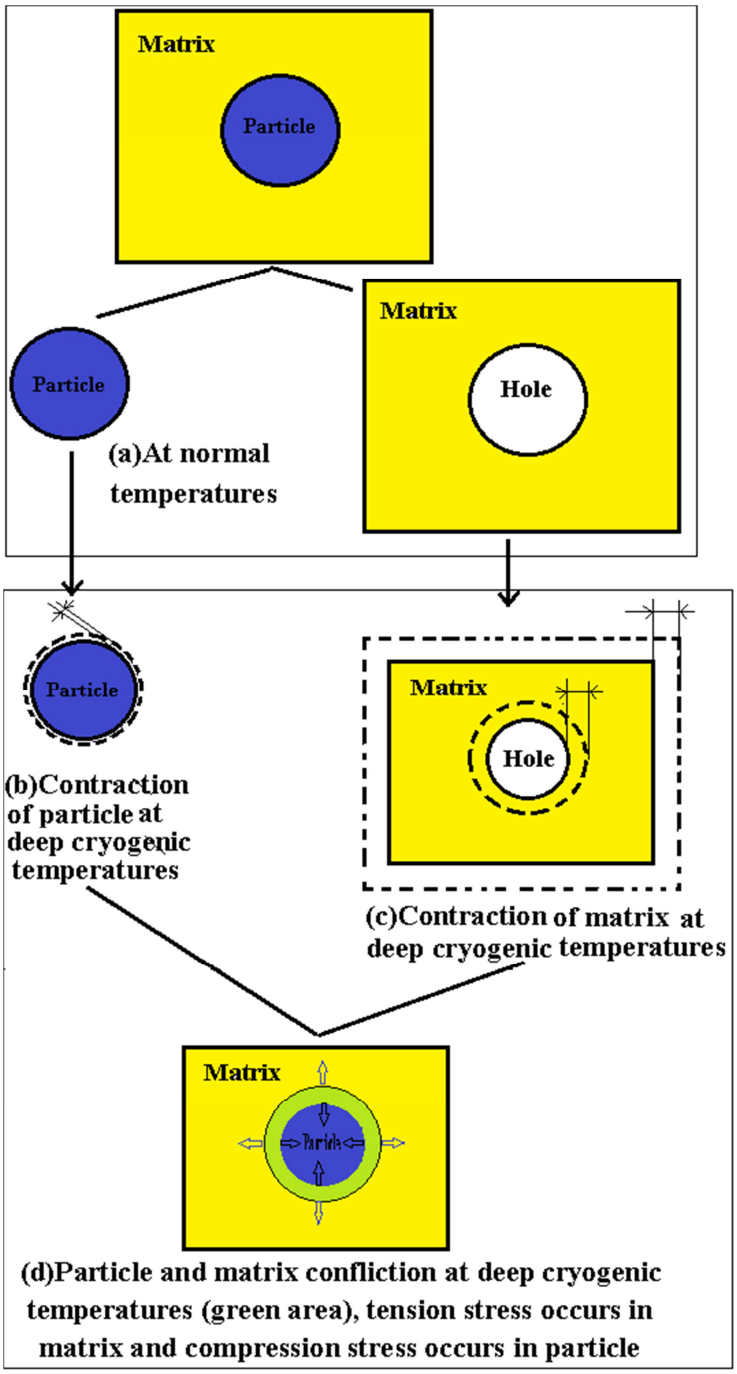

Figure 3. *Difference in contraction coefficient between primary carbide and matrix at deep cryogenic temperatures, a tension stress occurs.*

3. Materials and Method

Eight factors namely austenitizing, soaking and tempering temperatures; austenitizing, soaking and tempering times and finally, heating and cooling rates are parameters of DCT [27-29]. In this research work, tempering temperature (200°C), DCT temperature (-196°C), cooling rate (1.3°C/min), heating rate (5.5°C/min), and austenitizing temperature and time (900°C for 60 min) were kept constant. So, tempering and DCT soaking times would be the only parameters which could affect the parameters. Table 1 presents the chemical analysis of 45WCrV7 tool steel used in this study.

Table 1. *Chemical analysis of the 45WCrV7 tool steel.*

Element	(Wt%)	Element	(Wt%)	Element	(Wt%)	Element	(Wt%)	Element	(Wt%)	Element	(Wt%)
C	0.4800	Si	0.9950	Mn	0.3360	S	0.0250	P	0.0567	Fe	Balance
Cr	1.1200	W	1.5700	Ni	0.1280	Mo	0.0281	V	0.0148		

The temperature-time history is depicted in Figure 4.

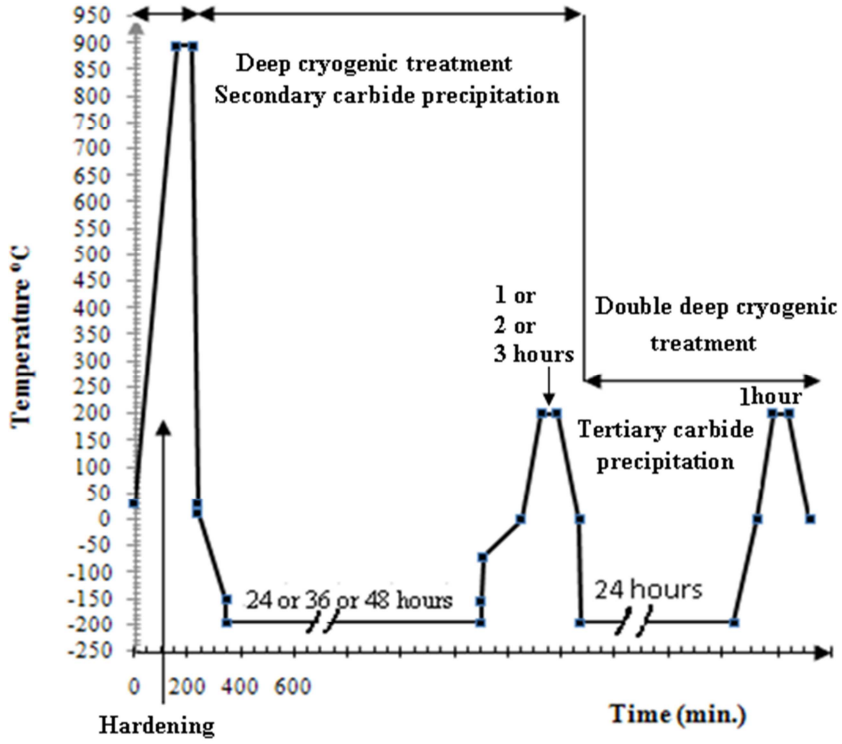

Figure 4. *The temperature-time history.*

The experimental procedure followed in this study is outlined in Figure 5.

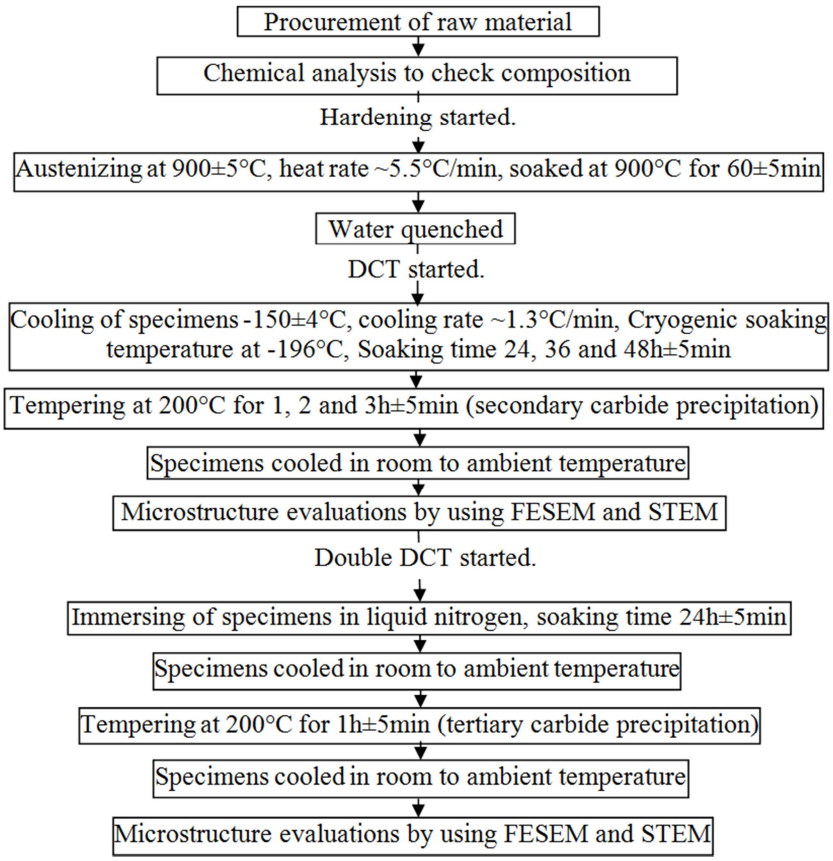

Figure 5. *Flow chart for experimental procedures.*

The specimens were given codes for easy identification during and after the experiments. The coding described in Table 2, Table 3 and Table 4. The coding procedure is as following:

(a) Cryogenically treated specimens:

The first two digits of the code for a cryogenically treated specimen indicate the soaking time (in hours) at -196°C. The last digit indicates the tempering time (in hours) at 200°C. For example, code 361, indicates a cryogenically treated specimen soaked at -196°C for 36 hours and tempered at 200°C for 1 hour.

(b) Double DCT specimens:

All of the specimens were immersed in liquid nitrogen for 24 hours in -196°C and then were tempered for 1 hour in 200°C. The first two digits of the code for a cryogenically treated specimen indicate the soaking time (in hours) at -196°C. The last digit indicates the tempering time (in hours) at 200°C. It separated by a dash after the cryogenically treated specimens. For example, code 361-241, indicates a cryogenically treated specimen soaked at -196°C for 36 hours and tempered at 200°C for 1 hour, then in subzero treatment it again has been DCT on -196°C for 24 hours and tempered on 200°C for 1 hour.

Table 2. *Codes for hardening of 45WCrV7 tool steel.*

Code	Process	Step 1	Step 2	Step 3	Tempering process
241, 242, 243, 361, 362, 363, 481, 482, 483	Water quenching	heated to 900±5°C (rate ~ 5.5°C/min)	soaked at 900°C for 60±5 min	Cooled in room to ambient temperature	Continued in Table 3

Table 3. *Codes for DCT of 45WCrV7 tool steel, first tempering; secondary carbide precipitation.*

Code	Cooling	Cryogenic temperature	Soaking time	Tempering temperature	Tempering time	Final cooling
241	-150±4 °C (rate ~1.3 °C/min)	-196±6°C	24 h		1 h	Cooled in room to ambient temperature
242					2 h	
243					3 h	
361			36 h		1 h	
362					2 h	
363					3 h	
481			48 h		1 h	
482					2 h	
483					3 h	

Table 4. *Codes for double DCT of 45WCrV7 tool steel, second tempering; tertiary carbideprecipitation.*

Code	Cooling	Soaking time	Tempering time	Final cooling
241-241, 242-241, 243-241, 361-241, 362-241, 363-241, 481-241, 482-241, 483-241	Immerse in liquid nitrogen	24 h	1 h	Cooled in room to ambient temperature

The cylindrical specimens were of 15 mm length and 12 mm diameter. To calculate each phasesizes and contents, at least five FESEM pictures were taken from five different scanned regions, using a 10^4 magnification, by using FESEM TESCAN MIRA II Machine. The reported contents are the average contents. The tertiary carbide, secondary carbide and primary carbide sizes and contents are measured by using phase analysis software, OLYSIA m^3. It was calibrated for images with 2048×1536 pixels.

JEOL ARM 200 atomic resolution microscope operated at 200 KV AppFive "Topspin" precession diffraction analysis machine (STEM). Theoretical patterns calculated for the phases according to ASTM 975-13 [30]. STEM specimens cut out as 3mm discs in wire cut machine, thinned to ~100nm by hand polishing, then dimpled and argon ion milled using a Gatan PIPS mill at cold stage. STEM machine used at LeRoyEyring Center for Solid State Science, John Cowley Center for HREM, Arizona State University, USA.

4. Results and Discussion

The microstructure results reported in Table 5.

Table 5. *Microstructure results.*

Specimen code	primary carbidecontentV%	secondary carbidecontentV%	secondary carbide and tertiary carbide contents V%	tertiary carbidecontentV%
241-241	0.42+0.20	2.18+0.11	3.1+0.15	0.92+0.05
242-241	0.47+0.15	2.42+0.12	3.2+0.16	0.78+0.04
243-241	0.37+0.20	3.73+0.16	4.4+0.22	0.67+0.03
361-241	0.57+0.05	4.69+0.23	5.3+0.26	0.61+0.03
362-241	0.60+0.05	6.92+0.35	7.4+0.36	0.48+0.02
363-241	0.34+0.20	8.91+0.45	9.3+0.46	0.39+0.02
481-241	0.35+0.20	10.04+0.50	10.3+0.51	0.26+0.01
482-241	0.25+0.20	12.66+0.63	12.9+0.65	0.24+0.01
483-241	0.24+0.20	12.87+0.64	13+0.65	0.13+0.01

The austenite to martensite transformation started (M_s) at 274.63°C and finished (M_f) at 59.63°C. M_s and $M_f$temperatures were obtained using Payson and Savage' Equations (2) and (3) [31-33], which are valid for 45WCrV7 tool steel.

$$M_s(°C) = 498.9 - (316.7×C\%) - (33.3×Mn\%) - (27.8×Cr\%) - (16.7×Ni\%-11.1×(Si+Mo+W)) \quad (2)$$

$$M_f(°C) = M_s(°C)-215 \quad (3)$$

Therefore retained austenite was completely transformed into martensite after DCT. After tempering of specimens, in terms of equilibrium state, martensite would be transformed to ferrite and carbides. These carbides can play the role of second phase in the matrix.

To verify the second mechanism of precipitation of carbides, the specimens have beenDCT again at -196°C for 24 hours, after which they were tempered at 200°C for 1 hour. Henceforth, this process will be called as double DCT. For the second mechanism of precipitation of carbides to be valid, new carbides (it is called tertiary carbide) should precipitate as the consequence of the double DCT around old carbides (primary and secondary carbides). It was observed that the content of the secondary carbide increased compared to the content before the double DCT. This means that the chemical compositions of the secondary carbide and the tertiary carbide are the same. The content of the tertiary carbide can be obtained by the subtraction of the content of the secondary carbide before and after the double DCT. As shown in Table 5, for specimen 241-241, the content of the secondary carbidebefore the double DCT was found to be 2.18 V% and after the double DCT it was increased to 3.1 V%, which means the content of the tertiary carbide is about 0.92 V%.

With an increase in soaking time, the metal matrix will become poorer in alloy elements and carbon content decreases. Therefore, after the double DCT, an increase in soaking time makes the precipitation of the tertiary carbide more difficult. This fact is clearly indicated in Table 5, with increase in cryogenic soaking time, the difference in the content of carbide before and after the double DCT (content of tertiary carbide) decreases.

The FESEM picture of backscattered electron image of the double DCT specimens is depicted in Figure 6(a) to Figure 6(d). As shown, a large number of tertiary carbide (white phases) surrounded the primary carbide (grey phases) and perhaps secondary carbide. Combining these results, and considering the fact that the content of tertiary carbide has increased with the double DCT (as shown in Table 5), the second mechanism of precipitation of carbideshas been verified again. But how canitexplain?

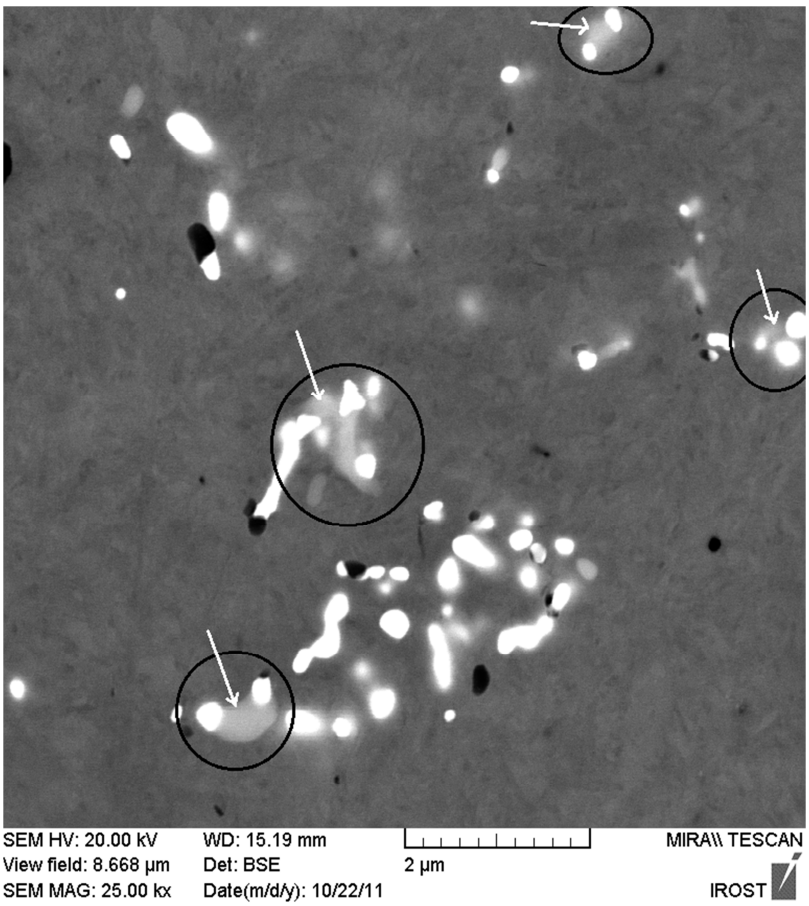

Figure 6(a). *Secondary carbides and tertiary carbides (white particles) surrounding the primary carbides, 241-241 specimen, FESEM.*

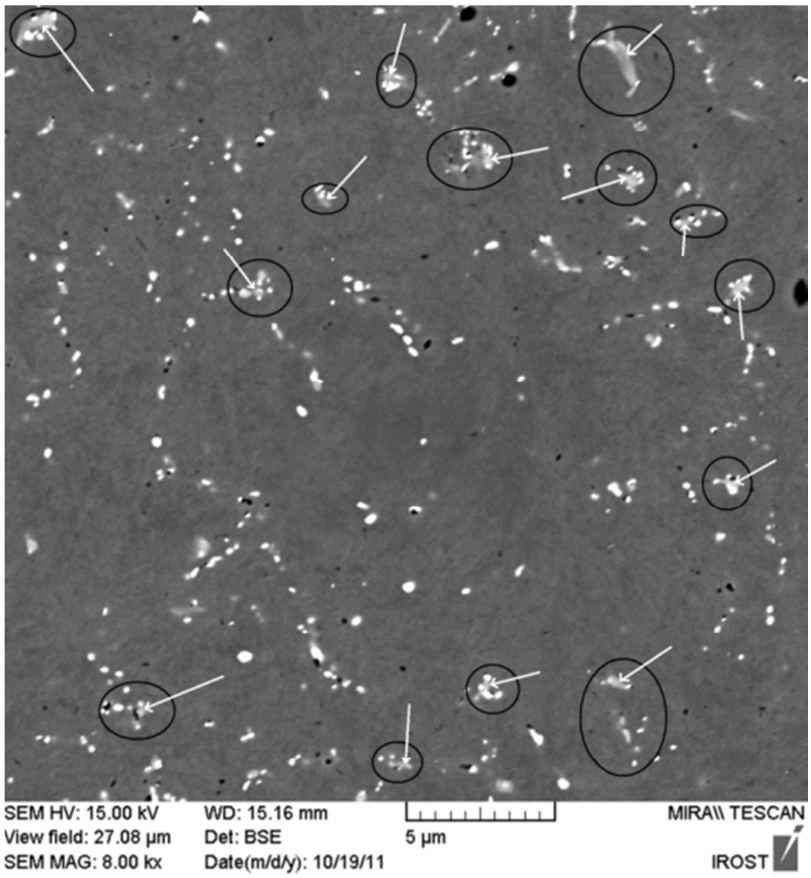

Figure 6(b). *Secondary carbides and tertiary carbides (white particles) surrounding the primary carbides, 362-241 specimen, FESEM.*

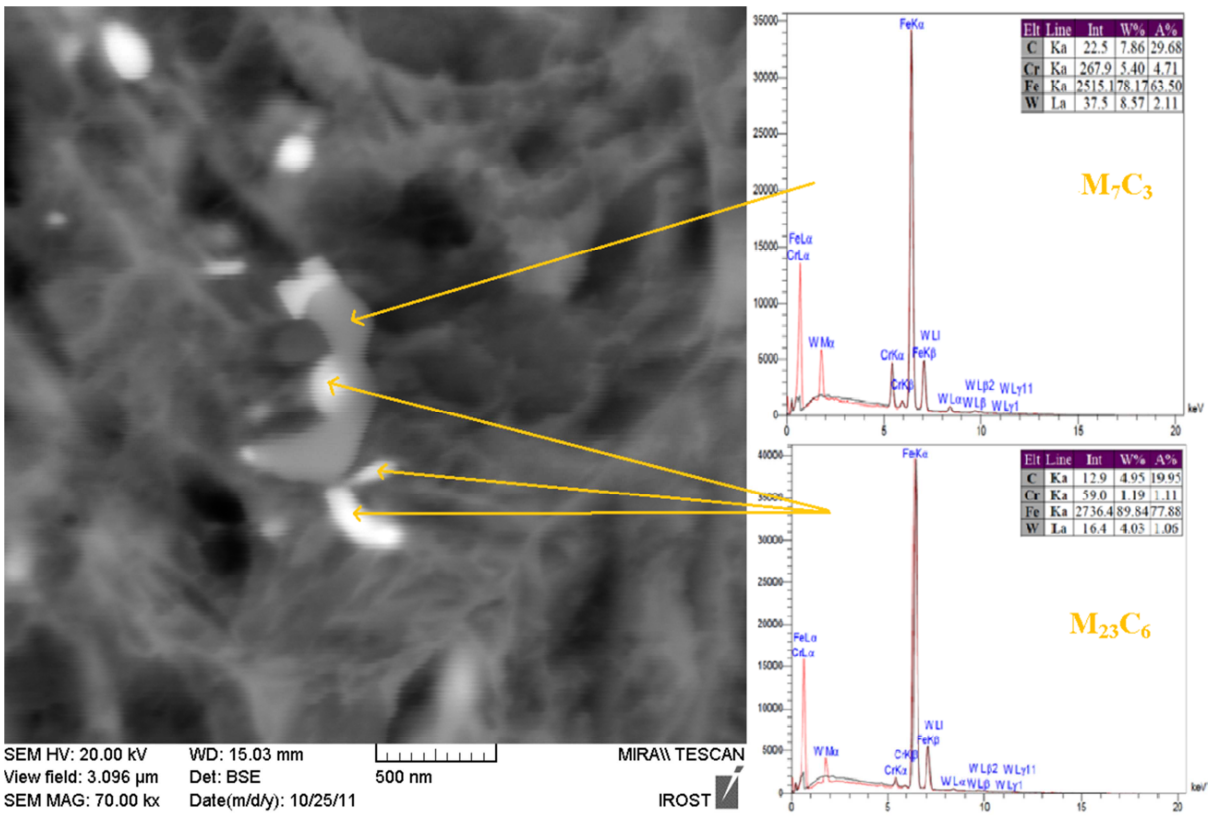

Figure 6(c). *Secondary carbides and tertiary carbides (white particles) surrounding the primary carbides, 241-241 specimen, FESEM.*

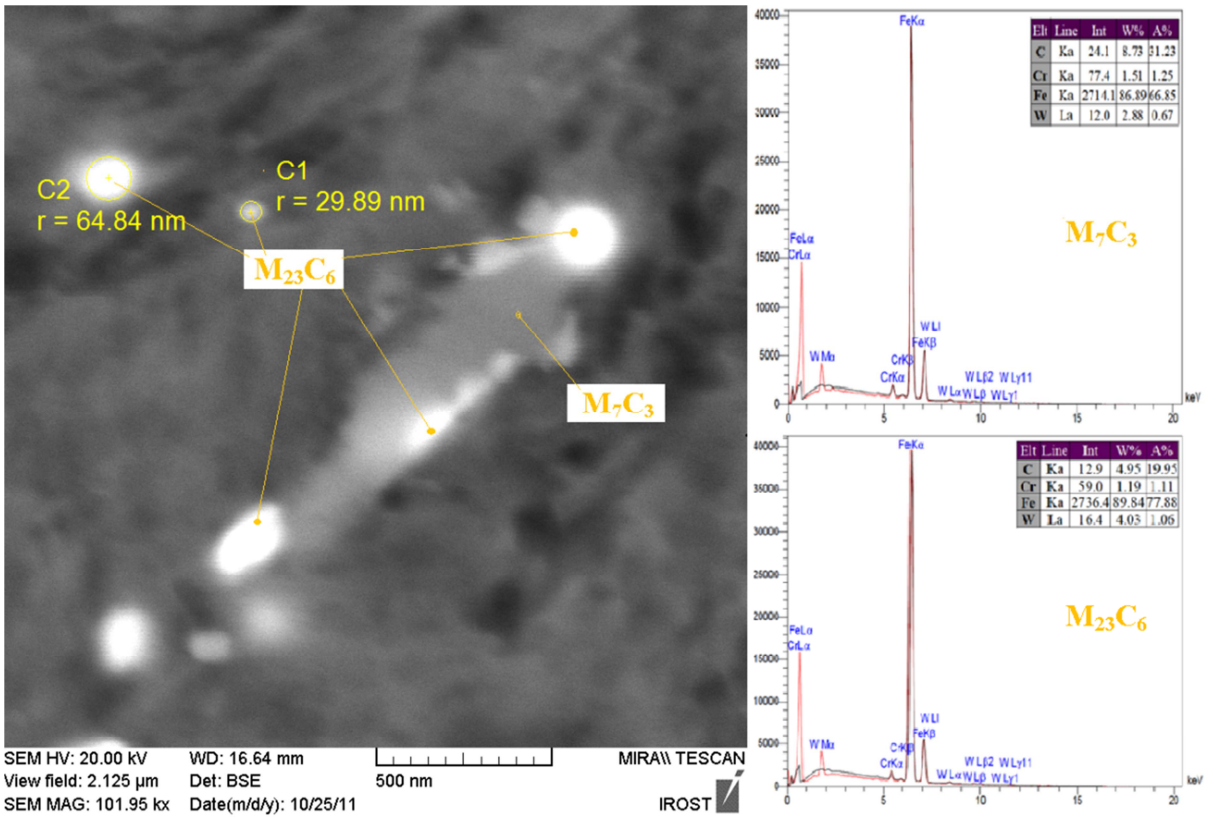

Figure 6(d). *Secondary carbides and tertiary carbides (white particles) surrounding the primary carbides, 361-241 specimen, FESEM.*

During solidification, large primary carbides precipitated in the grain boundaries and matrix. During austenizing, large primary carbides dissolve and led to smaller size. Therefore, the carbon and alloy concentrations increase around the primary carbides after quenching and before DCT. During DCT, the distortions are caused by difference in the thermal contraction between primary carbides and matrix. Consequently, with an increase in time, it produces more distortions and ultimately results in more dislocations. During tempering, carbon absorption occurred in these dislocations and, with an increase in time, carbon concentration surrounding the dislocations will increase, which facilitates the formation of more carbides.

According to second mechanism of precipitation of carbides, during DCT, around of primary carbideswill be preferred places for precipitation of carbides. At low tempering temperature, the diffusion is more difficult. Therefore how does it work?

Firstly, diffusion coefficient of carbon is higher than alloying element ones (such as W and Cr). Secondly, in grain boundaries, diffusion coefficient is higher than inside of grain. Because of grain boundary has higher defects than inside of grain [34]. All of these lead to facilitate precipitation of new carbidesaround the primary carbides in grain boundaries.

Figure 7 shows FESEM image of specimen 241-241 shows grain boundaries is more appropriate places for new carbides precipitation.

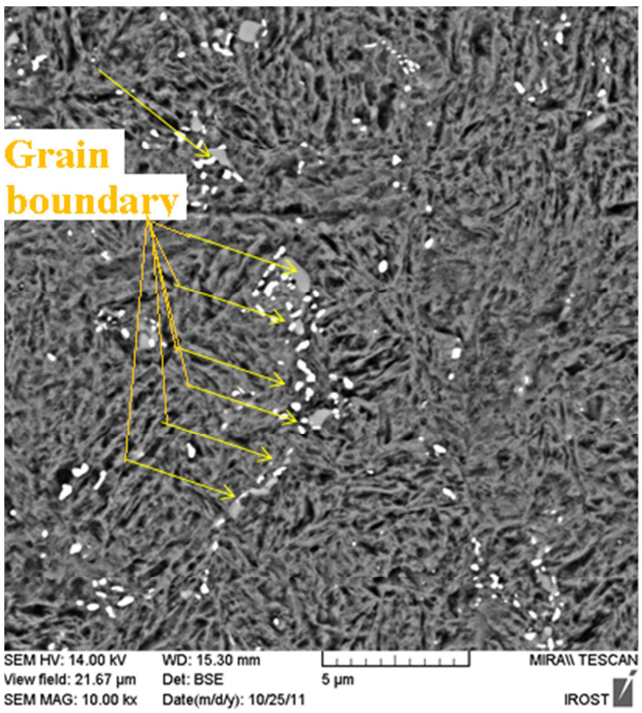

Figure 7. *Primary, secondary and tertiary carbides in the grain boundary, FESEM image for specimen of 241-241.*

Figure 8 shows STEM map of M_7C_3, $M_{23}C_6$, iron carbide, M_6C and Cr_3C_2 and nano-sized retained austenite in the ferrite matrix, taken from the same area about 80000 nm^2.

This method (STEM) detected ultra fine carbides.

Figure 8 shows secondary carbides and tertiary carbides (almost $M_{23}C_6$ and iron carbide) around the primary carbides (M_7C_3) with straight arrow. Therefore again, the preferred placesand second mechanism of precipitation of carbides has been verified experimentally by using STEM.

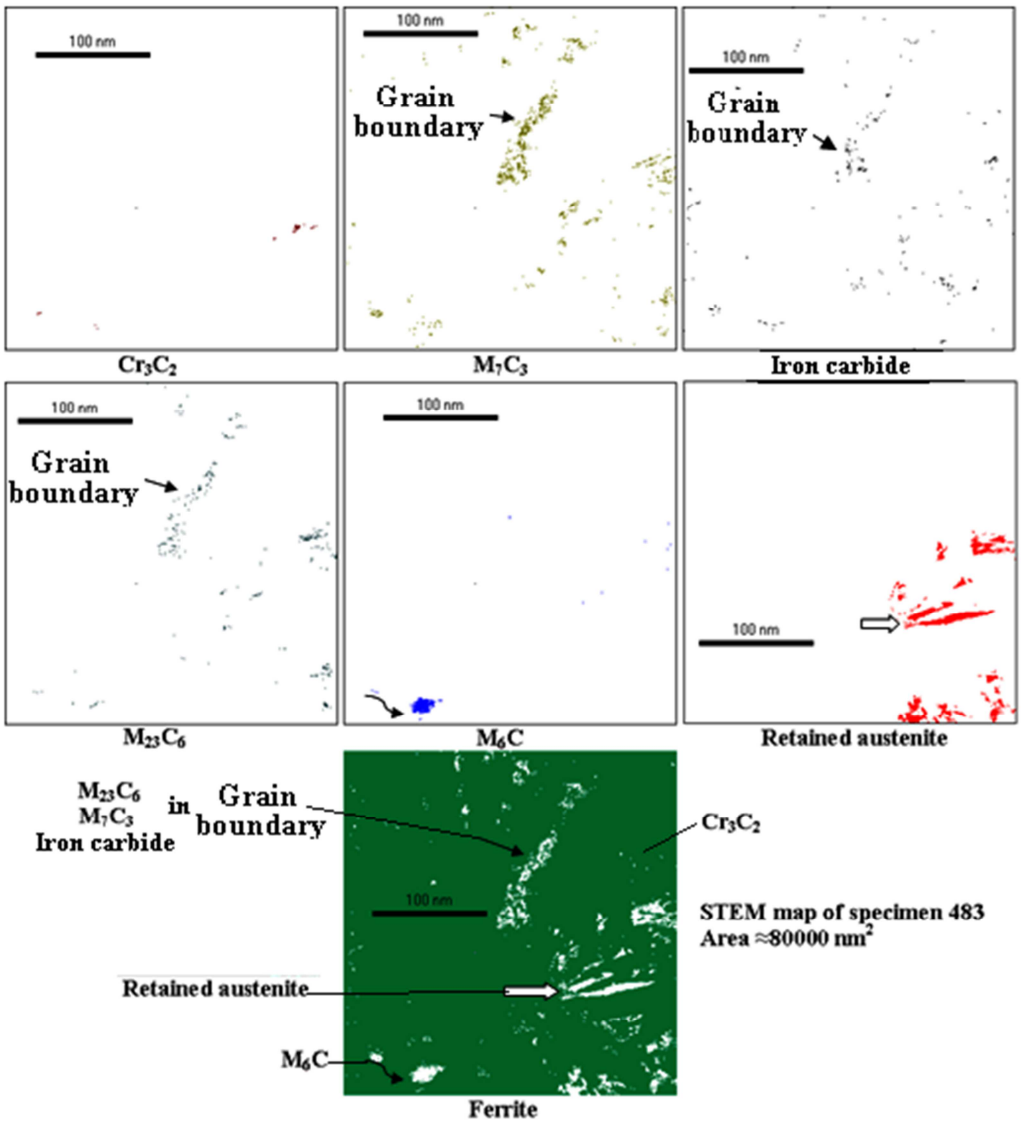

Figure 8. *STEM map of carbides for specimen of 483-241 shows secondary and tertiary carbides (almost $M_{23}C_6$ and iron carbides) around the primary carbides (M_7C_3) with straight arrow.*

5. Conclusions

In this research, nine sets of 45WCrV7 specimens have been DCT in -196°Cfor 24, 36, and 48 hours and have been tempered in 200°Cfor 1, 2, and 3 hours. Thenthey again have been DCT on -196°Cfor 24 hours and tempered on 200°C for 1hour. It is energetically favorable to form dislocations around carbides (due to thermal contraction differences between carbides and matrix) while holding tool steel at deep cryogenic temperatures following an austenite quench into water. During tempering, these dislocations serve to attract carbon atoms; which facilitates the formation of new carbides. FESEM, and STEM are provided to support presented model by examining samples subjected to different cryogenic holding times.

Glossary of Terms

Deep Cryogenic Treatment = DCT

FESEM = Field Emission Scanning Electron Microscopy

Primary Carbide = Carbide precipitates as the consequence of the solidification and they aren't dissolved after austenitization treatment.

Secondary Carbide = Carbide precipitates as the consequence of the first tempering.

STEM = Scanning Transmission Electron Microscopy

Tertiary Carbide = Carbide precipitates as the consequence of the second tempering.

XRD = X-Ray Diffraction

References

[1] S. E. Vahdat, S. Nategh, S. Mirdamadi, Microstructure and tensile properties of 45WCrV7 tool steel after deep cryogenic treatment, Materials Science and Engineering: A, 585 (2013) 444-454.

[2] S. Li, L. Deng, X. Wu, The mechanism investigation of deep cryogenic treatment on high alloy martensitic steel by low frequency internal friction, Cryogenics, 50 (2010) 433-438.

[3] S. Li, L. Deng, X. Wu, Y. a. Min, H. Wang, Influence of deep cryogenic treatment on microstructure and evaluation by internal friction of a tool steel, Cryogenics, 50 (2010) 754-758.

[4] S. Li, L. Deng, X. Wu, H. Wang, Y. a. Min, N. Min, Effect of deep cryogenic treatment on internal friction behaviors of cold work die steel and their experimental explanation by coupling model, Materials Science and Engineering: A, 527 (2010) 7950-7954.

[5] S. Li, N. Min, L. Deng, X. Wu, Y. a. Min, H. Wang, Influence of deep cryogenic treatment on internal friction behavior in the process of tempering, Materials Science and Engineering: A, 528 (2011) 1247-1250.

[6] S. Li, N. Min, J. Li, X. Wu, C. Li, L. Tang, Experimental verification of segregation of carbon and precipitation of carbides due to deep cryogenic treatment for tool steel by internal friction method, Materials Science and Engineering: A, 575 (2013) 51-60.

[7] J. Li, L. Tang, S. Li, X. Wu, Finite element simulation of deep cryogenic treatment incorporating transformation kinetics, Materials & Design, 47 (2013) 653-666.

[8] S. Li, N. Min, J. Li, X. Wu, Internal friction measurements of phase transformations during the process of deep cryogenic treatment of a tool steel, Cryogenics, 57 (2013) 1-5.

[9] Y. Shima, Y. Ishikawa, H. Nitta, Y. Yamazaki, K. Mimura, M. Isshiki, Y. Iijima, Self-Diffusion along Dislocations in Ultra High Purity Iron, MATERIALS TRANSACTIONS, 43 (2002) 173-177.

[10] H.-h. Liu, J. Wang, B.-l. Shen, H.-s. Yang, S.-j. Gao, S.-j. Huang, Effects of deep cryogenic treatment on property of 3Cr13Mo1V1.5 high chromium cast iron, Materials & Design, 28 (2007) 1059-1064.

[11] H.-h. Liu, J. Wang, H.-s. Yang, B.-l. Shen, S.-j. Gao, S.-j. Huang, Effect of Cryogenic Treatment on Property of 14Cr2Mn2V High Chromium Cast Iron Subjected to Subcritical Treatment, Journal of Iron and Steel Research, International, 13 (2006) 43-48.

[12] A. I. Tyshchenko, W. Theisen, A. Oppenkowski, S. Siebert, O. N. Razumov, A. P. Skoblik, V. A. Sirosh, Y. N. Petrov, V. G. Gavriljuk, Low-temperature martensitic transformation and deep cryogenic treatment of a tool steel, Materials Science and Engineering: A, 527 (2010) 7027-7039.

[13] D. Das, A. K. Dutta, K. K. Ray, Sub-zero treatments of AISI D2 steel: Part I. Microstructure and hardness, Materials Science and Engineering: A, 527 (2010) 2182-2193.

[14] D. Das, R. Sarkar, A. K. Dutta, K. K. Ray, Influence of sub-zero treatments on fracture toughness of AISI D2 steel, Materials Science and Engineering: A, 528 (2010) 589-603.

[15] G. Prieto, J. E. P. Ipiña, W. R. Tuckart, Cryogenic treatments on AISI 420 stainless steel: Microstructure and mechanical properties, Materials Science and Engineering: A, 605 (2014) 236-243.

[16] S. Li, Y. Xie, X. Wu, Hardness and toughness investigations of deep cryogenic treated cold work die steel, Cryogenics, 50 (2010) 89-92.

[17] J. J. Hoyos, J. M. Vélez, A. A. Ghilarducci, Comment on "Experimental verification of segregation of carbon and precipitation of carbides due to deep cryogenic treatment for tool steel by internal friction method" by Li et al. [Mater. Sci. Eng. A 575 (2013) 51–60], Materials Science and Engineering: A, 613 (2014) 1-2.

[18] P. Stark, B. L. Averbach, M. Cohen, Influence of microstructure on the carbon damping peak in iron-carbon alloys, Acta Metallurgica, 6 (1958) 149-155.

[19] I. Tkalcec, D. Mari, W. Benoit, Correlation between internal friction background and the concentration of carbon in solid solution in a martensitic steel, Materials Science and Engineering: A, 442 (2006) 471-475.

[20] H. K. D. H. Bhadeshia, S. R. Honeycombe, 5 - Formation of Martensite, in: H. K. D. H. B. R. Honeycombe (Ed.) Steels (Third Edition), Butterworth-Heinemann, Oxford, 2006, pp. 95-128.

[21] H. K. D. H. Bhadeshia, S. R. Honeycombe, 9 - The Tempering of Martensite, in: H. K. D. H. B. R. Honeycombe (Ed.) Steels (Third Edition), Butterworth-Heinemann, Oxford, 2006, pp. 183-208.

[22] H. K. D. H. Bhadeshia, C. M. Wayman, 9 - Phase Transformations: Nondiffusive, in: D. E. L. Hono (Ed.) Physical Metallurgy (Fifth Edition), Elsevier, Oxford, 2014, pp. 1021-1072.

[23] H. K. D. H. Bhadeshia, 21 - Physical Metallurgy of Steels, in: D. E. L. Hono (Ed.) Physical Metallurgy (Fifth Edition), Elsevier, Oxford, 2014, pp. 2157-2214.

[24] S. W. Ooi, P. Hill, M. Rawson, H. K. D. H. Bhadeshia, Effect of retained austenite and high temperature Laves phase on the work hardening of an experimental maraging steel, Materials Science and Engineering: A, 564 (2013) 485-492.

[25] H. K. D. H. Bhadeshia, Steels for bearings, Progress in Materials Science, 57 (2012) 268-435.

[26] D. Hull, D. J. Bacon, Introduction to Dislocations, Fourth ed., University of Liverpool, UK, 1988.

[27] K. Niaki, S. Vahdat, Optimization of Tensile Properties of AISI S1 Tool Steel, Trans Indian Inst Met, (2015) 1-5.

[28] S. E. Vahdat, S. Nategh, S. Mirdamadi, Effect of microstructure parameters on tensile toughness of tool steel after deep cryogenic treatment, International Journal of Precision Engineering and Manufacturing, 15 (2014) 497-502.

[29] S. E. Vahdat, Effect of deep cryogenic processing on tensile toughness of 45WCrV7 steel, International Journal of Steel Structures, 14 (2014) 571-578.

[30] A. S. T. M., E975, X-Ray Determination of Retained Austenite in Steel with Near Random Crystallographic Orientation, ASM International, Ohio, USA, 2013, pp. 1-7.

[31] W. Gestwa, M. Przylecka, D. S. MacKenzie, D. Pye, G. E. Totten, 29 - Heat treatment, in: W. F. Gale, PhD, P. T. C. Totemeier (Eds.) Smithells Metals Reference Book (Eighth Edition), Butterworth-Heinemann, Oxford, 2004, pp. 1-83.

[32] G. E. Totten, M. Narazaki, R. R. Blackwood, L. M. Jarvis, Failures Related to Heat Treating Operation, in: W. T. Becker, R. J. Shipley (Eds.) Failure Analysis and Prevention, ASM international, Ohio, 2002, pp. 210.

[33] W. G. Vermeulen, P. F. Morris, A. P. d. Weijer, S. v. d. Zwaag, Prediction of martensite start temperature using artificial neural networking, Ironmaking and Steelmaking, 23 (1996) 433-437.

[34] D. A. Porter, K. E. Easterling, Phase Transformation in Metals and Alloys, 3rd ed., Van Nostrand Reinhold Co. Ltd. (UK), Molly Millars Lane, Wokingham, Berkshire, England, 1983.